

Design and Control of a Simplified NIBS PFC Converter Using Grasshopper-Optimized PI Controller for Battery Charging in Defence Applications

K.M. Vijayalakshmi* and M.G. Umamaheswari

Department of Electrical & Electronics Engineering, Rajalakshmi Engineering College, Chennai - 602 105, India

**E-mail: vijayalakshmi.km@rajalakshmi.edu.in*

ABSTRACT

This research focuses on the design and analysis of transformerless single-stage power architecture for charging Light Electric Vehicle (LEV) batteries, offering an alternative to conventional low or high-frequency transformer-based methods. Diode bridge rectifier (DBR) losses are the primary cause of lower efficiency in traditional Power Factor Correction (PFC) circuits used for battery charging. In this article, a single-phase AC to DC Non-Ideal Bridgeless SEPIC Converter (NIBS) has been designed and controlled for PFC and output regulation for battery charging in defence applications. Establishing a reliable and scalable EV charging infrastructure is pivotal to harnessing the full potential of LEVs in defence, improving operational efficiency, and enhancing energy security. A Hankel Matrix Method is employed to simplify the seventh-order model of the NIBS converter to third-order model. The efficacy of the NIBS converter-based charger is illustrated with the help of simulation-based performance under rated and over wide fluctuations in AC mains voltage, load and set point. It provides an efficiency of 91.99 %, input power factor of 0.9996, and THD of 2.34 % for rated load.

Keywords: Power Quality(PQ); Power Factor Correction (PFC); Battery Charger (BC); Non-Ideal Bridgeless Single Ended Primary Inductance Converter (NIBSEPIC); Grasshopper Optimization Algorithm(GOA); Total Harmonic Distortion(THD); State Space Averaging (SSA); Genetic Algorithm(GA); Particle Swarm Optimization (PSO)

NOMENCLATURE

UPF	: Unity Power Factor
CC/CV	: Constant Current/Constant Voltage
AC	: Alternating current
DC	: Direct Current,
PI	: Proportional Integral
SMPS	: Switched Mode Power Supply
UAV	: Unmanned Aerial Vehicles
EV	: Electric Vehicles
PWM	: Pulse Width Modulator.

1. INTRODUCTION

The need for alternate fuel sources and to prevent further greenhouse gas emissions in the atmosphere is pushing the automotive industry to shift gradually to electrified vehicles. Electrification of light utility vehicles is considered to be one of the critical driving factors towards achieving the “Sustainable Development Goals (SDG)” promulgated by the “United Nations (UN)” among all its member states. Improving the power efficiency endows the stakeholders of vehicle electrification projects, with a means to comply with the “Clean and Green Energy” regulations imposed by national bodies towards aligning with SDG. Applications for electric vehicles are extremely limited in most countries, despite their significant advantages over conventional Internal

Combustion (IC) engines. Currently, the absence of sufficient infrastructure for charging is the main obstacle faced by the EV industry. Because battery-powered vehicles¹⁻⁴ only run on electricity, they are the most widely used type of EV in the market. Batteries are indispensable in defence applications due to their portability, reliability, and ability to provide continuous power in various conditions. They support a wide range of defence technologies, from communication devices and UAVs to wearable tech and advanced weapon systems. Continuous advancements in battery technology are crucial in meeting the evolving power needs of modern defence operations. Maintaining a Unity Power Factor (UPF) in battery systems used in defence applications particularly is vital for several reasons. To ensure the quality of input power in accordance with international standards, power electronics circuits that control voltage for battery energy storage systems should be suitably constructed. In single-stage active power factor correction circuits, Switched-Mode Power Supplies (SMPS) are employed⁵.

These single-stage PFCs are employed to control the input power factor and output voltage that result from the introduction of nonlinearities provided by switching devices. This correction aids in reducing harmonic contents in the source current by preserving UPF at the source side and providing tight load voltage regulation. Various PFC converter circuits have been employed previously to achieve UPF control. Formerly, PFC circuits used a dual-stage to attain output voltage regulation and UPF but they suffered from pitfalls such as larger size,

higher cost, and lower efficiency. In recent times, single-stage AC-DC converters have been favoured because they need less number of devices and provide high efficacy. They utilize switching power converters with control circuitry that forces supply current to mimic supply voltage, effectively emulating a resistor. As a result, the choice of a PFC converter for EV chargers involves optimizing component reliability against component quantity.

The chosen trade-off achieves SAE J1772 standards⁶ for power density and efficiency. Compared to conventional PFC topologies, bridgeless topologies offer reduced conduction loss, and higher efficiency at lower line voltages, since the DBRs are absent. Figure 1 below illustrates the impact of DBR (diode break-over voltage) in the conventional SEPIC, leading to an increase in the displacement factor (a decrease in power factor) at the zero-crossing point of the source current, compared to the NIBS converter.

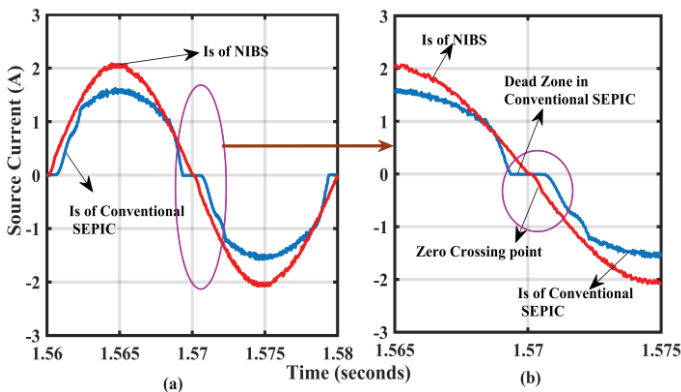


Figure 1. Comparison of Source currents of Conventional SEPIC and NIBS Converter, (a) Source currents; and (b) Magnified view of zero crossing of source currents.

DC-DC Boost converters⁷⁻⁸ are highly advantageous in PFC applications due to their ability to improve power factor, reduce harmonics, achieve high efficiency, and handle a wide range of input voltages. Their compact design, cost-effectiveness, scalability, and advanced control features make them an essential component in modern power electronics, ensuring compliance with regulatory standards and contributing to overall energy efficiency and reliability. Buck converters⁹ offer numerous advantages in battery charging applications, including high efficiency, stable and regulated output, wide input voltage range, compact size, fast and controlled charging, enhanced safety features, cost-effectiveness, scalability, and low electromagnetic interference. Buck-boost converters offer significant merits in both PFC and battery charging utilizations due to their capacity to handle a wide variety of input voltages, high efficiency, compact size, versatile voltage conversion, and enhanced safety features¹⁰⁻¹¹. The Cuk converter performs buck and boosts mode but with inverted output polarity, so the SEPIC surrogates the Cuk converter with positive output¹²⁻¹³.

Step-up and step-down features of conventional SEPIC converters are mostly used for instantaneous line current shaping along with load voltage regulation in PFC rectifiers¹⁴⁻¹⁶. It provides a load voltage that depends on the duty ratio of the PWM signal. Various advantages offered by a SEPIC converter are easy implementation, transformer

isolation, less Electromagnetic Interference (EMI), natural short circuit protection and best steady-state operation. The existence of inductors on both the input and output sides, also offers continuous input and output currents with minimal current ripples. These advantages make them suitable for a wide variety of applications where traditional converters may fall short. Recently, bridgeless topologies PFC converters are gaining attention due to low conduction losses, because of the elimination of front-end DBR in conventional PFC converters like Boost, Cuk and SEPIC converter. Figure 1 explains the dead zone in a conventional one.

A bridgeless AC-DC PFC is used in battery charging applications to improve efficiency by minimizing the number of components and power losses typically associated with the rectification process. Compact Design and improved thermal performance are added advantages of bridgeless converters¹⁴⁻¹⁷. CC/CV charging with integrated PFC enhances EV battery charging effectiveness and overall charger performance when implementing bridgeless isolated configuration of SEPIC converter. Non-isolated NIBS converter operating in Continuous Current Conduction Mode (CCM) is considered here.

The battery charger that is being presented here is designed using a NIBS PFC AC-DC converter, which guarantees a significant improvement in PQ indices at supply AC mains. It also provides necessary battery charging¹⁴⁻¹⁷ current profile over a broader range of various operating conditions. Additionally, the complexity and cost of the charging system are all optimized by the transformer-less voltage gain adjustment approach. Besides, CCM operation reduces ripple currents, Electromagnetic Interference (EMI), and better performance in PFC, and lower Peak Currents. In concise terms, major improvements made possible by this NIBS PFC architecture are summarized as follows.

- This configuration eliminates input side diodes. As a result, during one switching interval, fewer components receive current
- The input inductor and switch configuration eliminates the need for an input-side filter
- Both switches have an identical gating sequence, which makes control simple
- Overall conduction loss is reduced due to the elimination of DBR.

NIBS converter is a seventh-order AC-DC converter. To reduce the computational complexity of higher-order dynamic systems, various model order reduction techniques have been suggested in the literature. To simplify the order NIBS converter, the Hankel matrix order reduction approach¹⁸⁻¹⁹ is chosen due to its computational efficiency for higher-order systems. Various controllers implemented previously and comply with global benchmarks like IEC 61000-3-2²⁰. The choice of control technique for voltage regulation and input current shaping depends on various factors, like specific application requirements, and complexity, cost, and performance characteristics. Optimization control algorithms²³⁻²⁷ provide significant advantages over conventional control techniques²¹⁻²² by enhancing performance and robustness, handling complex

multi-objective scenarios, and offering predictive capabilities. Their adaptability, scalability, and ability to integrate with modern technologies make them appropriate for diverse applications, such as industrial automation, energy management and advanced manufacturing. By leveraging these benefits, systems can achieve superior operational efficiency, cost savings, and improved overall performance. The Grasshopper Optimization Algorithm (GOA)²³⁻²⁵ is employed to determine the optimum parameter values of the PI controller. The other optimization techniques like GA and PSO²⁶⁻²⁷ have been implemented for tuning PI controller.

The Grasshopper Optimization Algorithm (GOA) is chosen over other optimization techniques due to its unique advantages in handling complex, nonlinear, and multi-objective problems. Also GOA excels in balancing **exploration** and **exploitation**, which are critical for avoiding local optima and effectively identifying the global optimum. GOA's capability to efficiently handle such multi-objective functions ensures enhanced transient response and reduced steady-state error.

This research work is structured as follows: Subsection 2 dispenses with working, design, and closed-loop control of the NIBS converter. Subsection 3 demonstrates the

design of GOA-tuned outer voltage and inner current PI controllers. Simulation results of the NIBS converter have been represented in subsection 4 for battery charging. It also includes a performance analysis of the NIBS converter for different operating conditions. Subsection 5 discusses the hardware implementation of the NIBS Converter. Subsection 6 discusses the conclusion.

2. NON IDEAL BRIDGELESS SEPIC CONVERTER

Figure 2 depicts a NIBS converter, constructed by paralleling two SEPIC converters, with each dedicated to each half cycle of source voltage, V_{in} . NIBS converter is a seventh-order converter as it has seven energy storage elements, such as four inductors (L_1 , L_2 , L_{01} and L_{02}), and three capacitors (C_1 and C_2 and C_o). S_1 and S_2 are active high-speed MOSFET switches. D_p and D_n are slow-recovery diodes, which operate on supply frequency. D_{01} and D_{02} are two Schottky diodes which operate on switching frequency. V_o is the terminal voltage across the resistive load (R_L). r_{L1} , r_{L2} , r_{L01} , r_{L02} , r_{C1} , r_{C2} , r_{S1} , r_{S2} , r_{D01} , r_{D02} , and r_{Co} represent parasitic elements of the NIBS Converter, respectively. Figure 3 represents the different modes of operation of the NIBS converter during one input cycle of the source voltage.

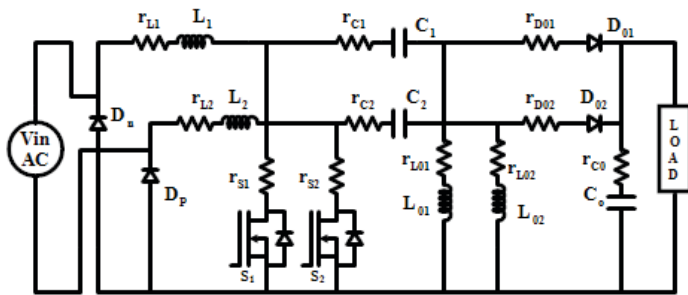


Figure 2. Circuit of 1Φ AC-DC NIBS converter.

2.1 Design of 1Φ AC-DC NIBS Converter

The 1Φ AC-DC NIBS converter components are calculated with the following specifications: Source voltage is (V_{in}) - 60 V, switching speed (f_s) - 50 kHz, duty ratio (D) - 0.67, desired output load voltage V_o - 100V, load resistance is 50 Ω, and output current through load - 2A. Desired variation in the inductor currents and the capacitor voltages considered for designing components is as follows: ΔI_{L1} and ΔI_{L2} : 2.8 % of input current; ΔI_{L01} and ΔI_{L02} : 2.8 % of input current; ΔV_{C1} and ΔV_{C2} : 4 % of output voltage (V_o); and ΔV_{Co} : 0.2% of load

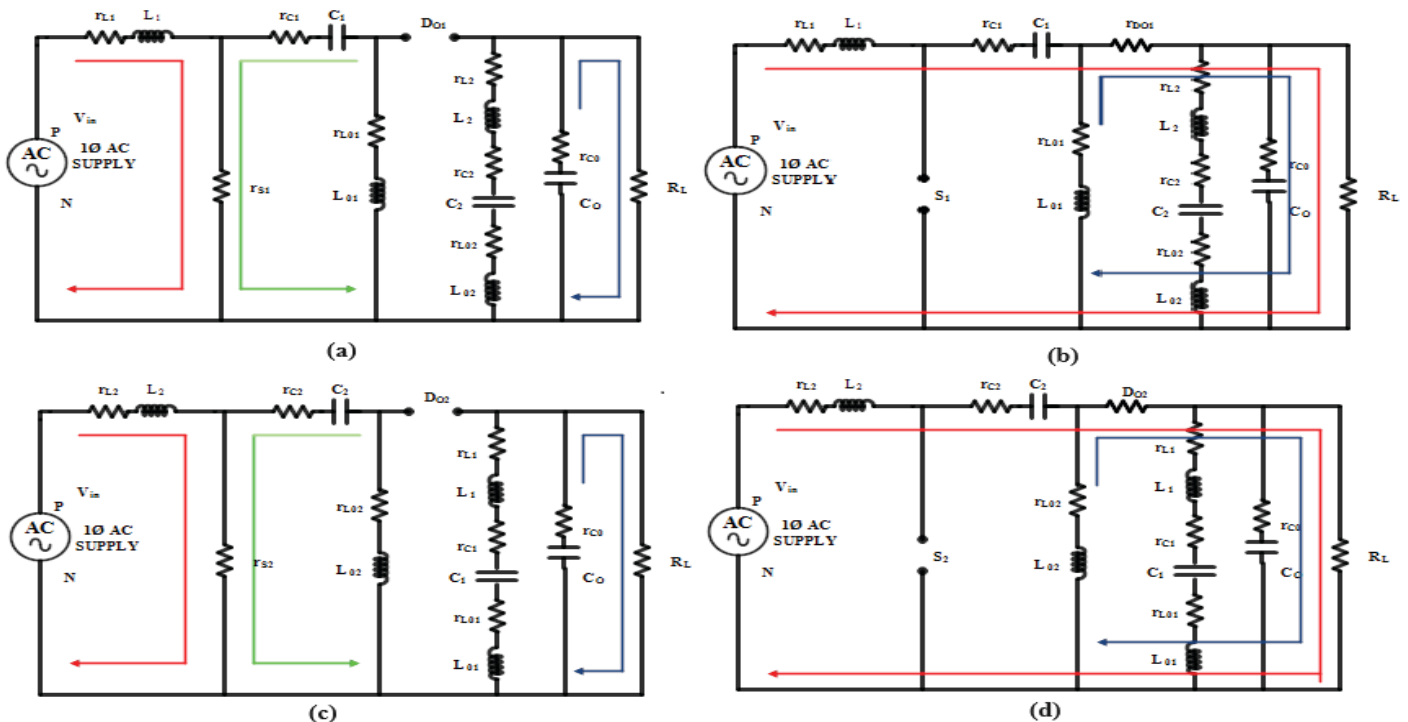


Figure 3. Modes of operation of NIBS converter.

Table 1. Parasitic components value of NIBS Converter

Parasitic resistance	$r_{L1}(\text{m}\Omega)$ & $r_{L2}(\text{m}\Omega)$	$r_{s1}(\text{m}\Omega)$ & $r_{s2}(\text{m}\Omega)$	$r_{L01}(\text{m}\Omega)$ & $r_{L02}(\text{m}\Omega)$	$r_{D01}(\text{m}\Omega)$ & $r_{D02}(\text{m}\Omega)$	$r_{C1}(\text{m}\Omega)$ & $r_{C2}(\text{m}\Omega)$	$r_{Co}(\text{m}\Omega)$
Value	12.5	1	12.5	1	10	10

voltage (V_o). Calculated values of inductor and capacitor for a power output of 200 W NIBS converter are given by the following design Eqn. (1) - (4).

$$L_1 = L_2 = \frac{V_n * D}{f_s \Delta I_L} = 4. \text{ mH} \quad (1)$$

$$L_0 = L_0 = \frac{V_n * D}{f_s \Delta I_b} = 2. \text{ mH} \quad (2)$$

$$C_1 = C_2 = \frac{V_o * D^2}{R_L * f_s * \Delta V_C * (1-D)} = 150 \mu\text{F} \quad (3)$$

$$C_o = \frac{V_o * D}{R_L * f_s * \Delta V_{C_o}} = 10000 \mu\text{F} \quad (4)$$

The parasitic resistances connected with each component of the NIBS converter are listed in Table 1.

2.2 Transfer Function of 1 ϕ AC-DC NIBS Converter

The state space model of a 1 ϕ AC-DC NIBS converter is arrived at by taking $S = 1$ when the MOSFET is ON, and $S = 0$ when the diode is ON. MOSFET switches (S_1 and S_2) and diodes (D_{01} and D_{02}) have been modelled by considering their conduction loss. MOSFET switches S_1 and S_2 have their on-state resistance as r_{s1} and r_{s2} and the on-state resistance of diodes as r_{d01} and r_{d02} . Since the NIBS converter has seven passive components, it can be modelled as a seventh-order dynamic system. Parasitic elements of inductors and capacitors are also considered while modelling the converter. SSA technique is applied to derive equivalent matrices of state transition matrix A , input matrix B , output matrix C , and feed-forward gain matrix E (which is 0 here) for the system. Assume D as the duty cycle for modes I and III and $(1-D)$ as the duty ratio for modes II and IV.

The transfer function can be found from following expression:

$$\begin{bmatrix} G_{id(s)} \\ G_{vd(s)} \end{bmatrix} = C * (SI - A)^{-1} B_d + E_d \quad (5)$$

where, A , B_d , C , and E_d represent final equivalence matrices for the NIBS system obtained by applying Kirchoff's laws and writing the mode Eqn.

Achieving unity power factor and load regulation necessitates a closed-loop control system. Resultant seventh-order transfer functions for $G_{vd(s)}$ and $G_{id(s)}$ are derived as following Eqn. (6) and Eqn. (7):

$$G_{vd(s)} = \frac{(-15.92 s^6 + 4.233 \times 10^4 s^5 + 2.138 \times 10^8 s^4 + 2.784 e11 s^3 + 1.725 e14 s^2 + 4.297 e16 s - 7.143 e18)}{(s^7 + 3880 s^6 + 6.853 e06 s^5 + 7.254 e09 s^4 + 4.834 e12 s^3 + 1.952 e15 s^2 + 4.011 e17 s + 1.567 e18)} \quad (6)$$

$$G_{id(s)} = \frac{1.894 e05 s^6 + 5.831 e08 s^5 + 7.208 e11 s^4 + 4.716 e14 s^3 + 1.515 e17 s^2 + 6.555 e18 s + 2.404 e19}{s^7 + 3880 s^6 + 6.853 e06 s^5 + 7.254 e09 s^4 + 4.834 e12 s^3 + 1.952 e15 s^2 + 4.011 e17 s + 1.567 e18} \quad (7)$$

The designed system's closed-loop control demands monitoring of seven state variables, comprising i_{L1} , i_{L2} , i_{L01} , i_{L02} , V_{C1} , V_{C2} , and V_{Co} . This brings complexity to controller design and increases the number of sensors involved. By retaining the dominant poles associated with output capacitor voltage (V_{Co}) and input inductor currents (i_{L1} , i_{L2}) and neglecting the less influential state variables, the seventh-order model is simplified to a required third-order representation, using the Hankel matrix reduction approach, a state-space based approach. The reduced transfer function of the NIBS converter, $G_{red}(s)$ is,

$$G_{red(s)} = \frac{5.831 \times 10^8 s^2 + 7.208 \times 10^{11} s + 4.716 \times 10^{14}}{s^3 + 3880 s^2 + 6.853 \times 10^6 s + 7.254 \times 10^9} \quad (8)$$

2.3 Closed-Loop Control of NIBS Converter

Figure 4 explains the closed-loop implementation of the AC-DC NIBS converter using GOA-tuned outer and inner PI controllers. This segment presents the implementation of a closed-loop control technique for shaping source current I_s and regulating the output of an NIBS converter operating as a PFC and a battery charger. The battery voltage/battery current is measured, compared with the nominal battery voltage/discharge current and voltage error/current error is routed to GOA tuned PI outer controller. Outer GOA-tuned PI controller governs battery voltage/battery current based on State of Charge (SoC) and generates a reference current for the inner loop. The sum of input inductor currents (i_{L1} and i_{L2}) is compared to a reference current, and the resulting error is fed into a GOA-tuned inner PI current controller. The controller's output drives a PWM generator, which produces pulses to control the MOSFET gates.

3. DESIGN OF OUTER AND INNER GOA TUNED PI CONTROLLER

To achieve the desired output and to avoid corruption of source current, GOA tuned PI controller is chosen as it minimises steady-state error and boosts stability. Proportional gain (K_p) and integral gain (K_i) for both voltage and current controllers are determined using the GOA method. The GOA can be adapted to minimize error in various applications, such as parameter tuning in control systems, machine learning model training, or any optimization challenge where the goal is to minimize an error function and maximize the fitness function.

The fitness function is determined using the Integral Time Absolute Error (ITAE) performance criterion. GOA then

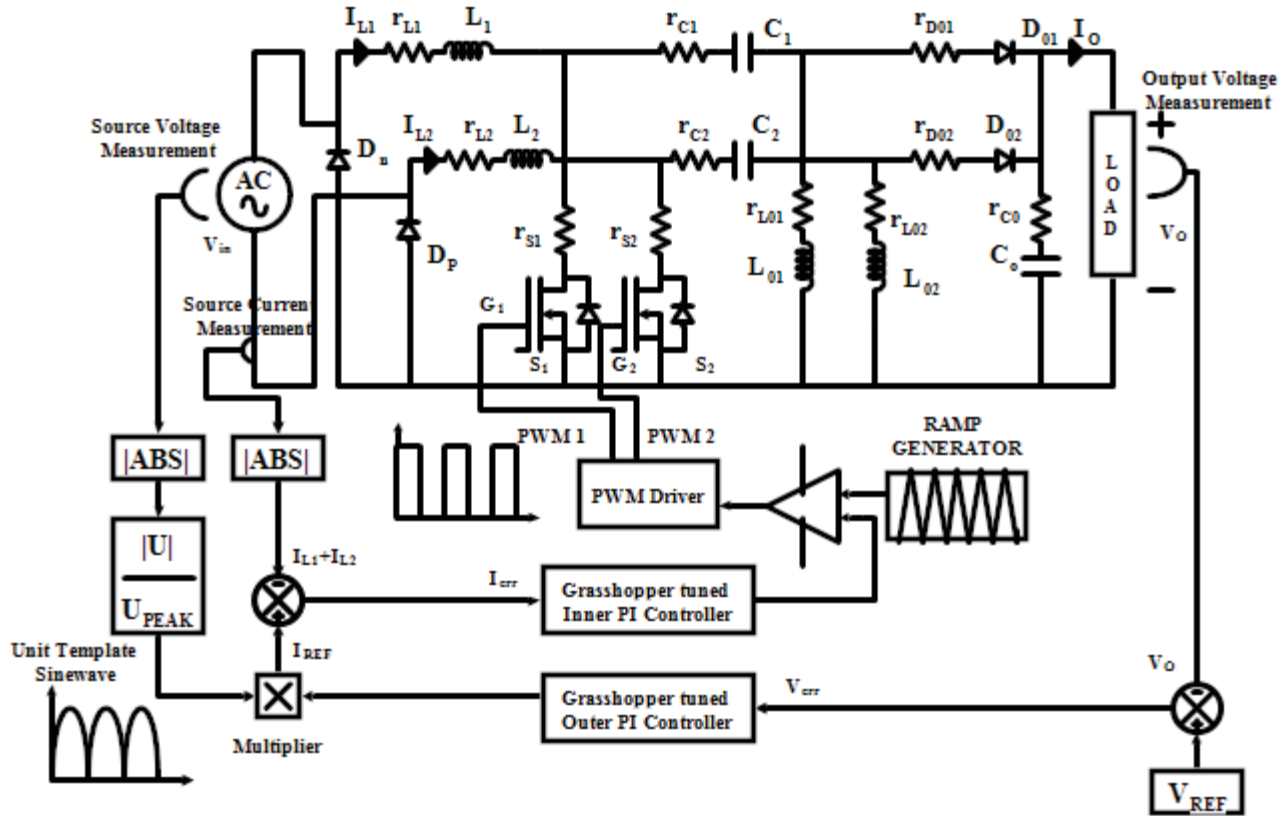


Figure 4. Control of NIBS converter using GOA-tuned outer and inner PI controller.

refines this fitness function so that optimized K_p and K_i values result in a reduction of voltage and current errors as well as harmonic contents. Thus, the power factor achieves close to unity with less % THD. This computation is performed for every member of the GOA population. Figure 5 explains the steps involved in the GOA optimization process.

The optimal design of K_p and K_i for both outer voltage and inner current PI controllers are obtained to be 0.1 and 1, respectively, using the GOA optimization algorithm. A closed-loop simulation of the NIBS converter has been done with these obtained values. Specifications for the GOA algorithm are outlined in Table 2.

Table 2. Simulation variables of GOA

Name of the variable	Data
Overall population size (Grasshoppers count)	50
Maximum iteration count (Max_Iter)	100
No. of dimensions (P)	2
No. of steps	10
Acceleration constants (K_1, K_2)	1.798
Inertial mass, (M_{max}, M_{min})	0.8, 0.5
Span of K_p	0.0-1.0
Span of K_i	1-10

4. SIMULATION RESULTS

To examine the performance of the NIBS PFC-based battery charger, the converter is simulated using MATLAB/Simulink software tool. Lithium-ion (Li-ion) batteries, renowned for their high energy density, longevity, and minimal self-discharge, are widely employed in various charging

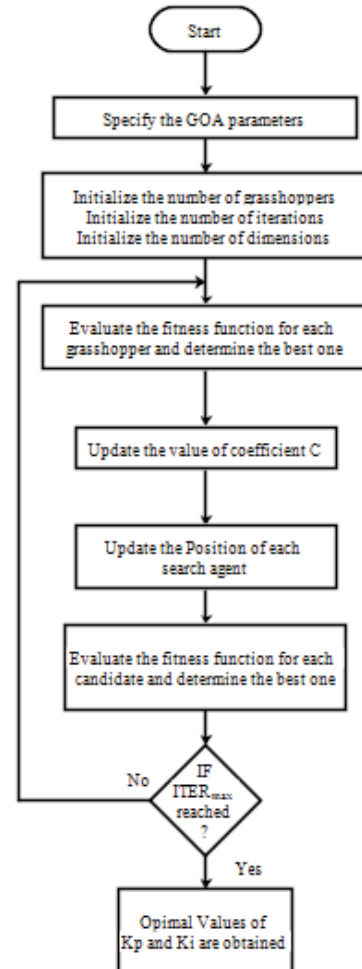


Figure 5. Flow chart for GOA.

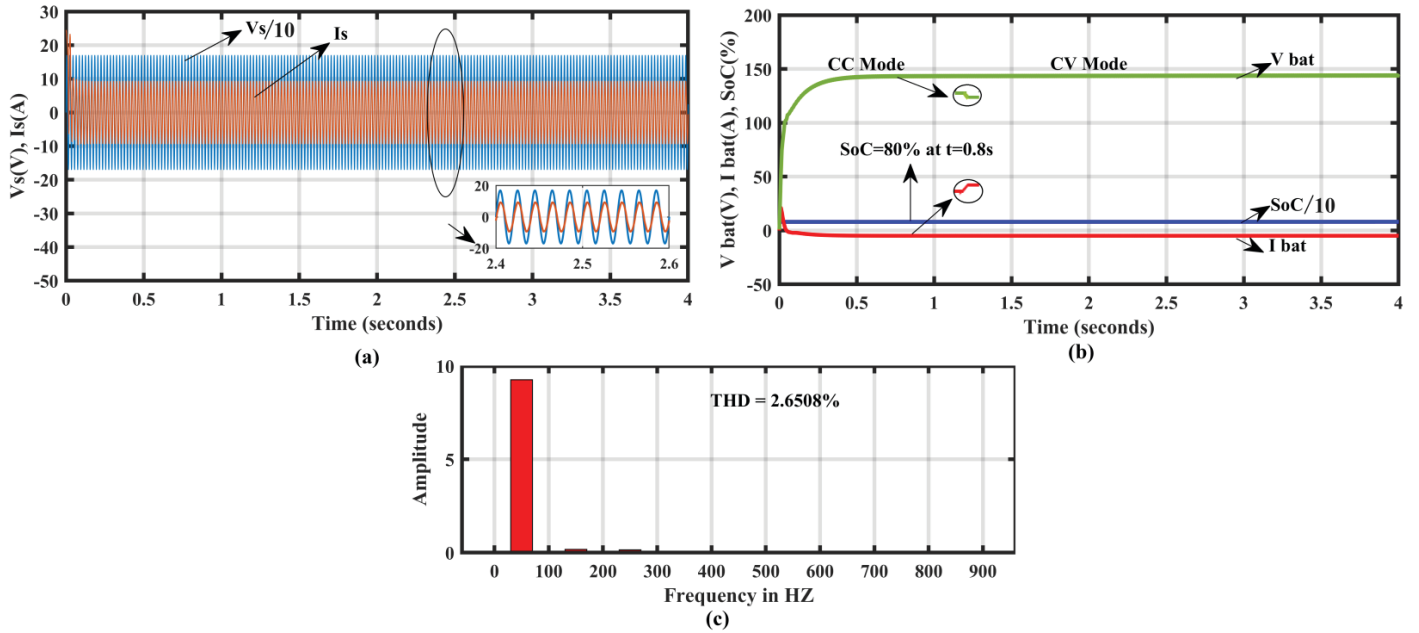


Figure 6. Simulation Results of Battery under Nominal Conditions (a) Source voltage and source current; (b) Battery voltage, battery current and State of Charge (SoC) under nominal condition; and (C) THD spectrum of the source current.

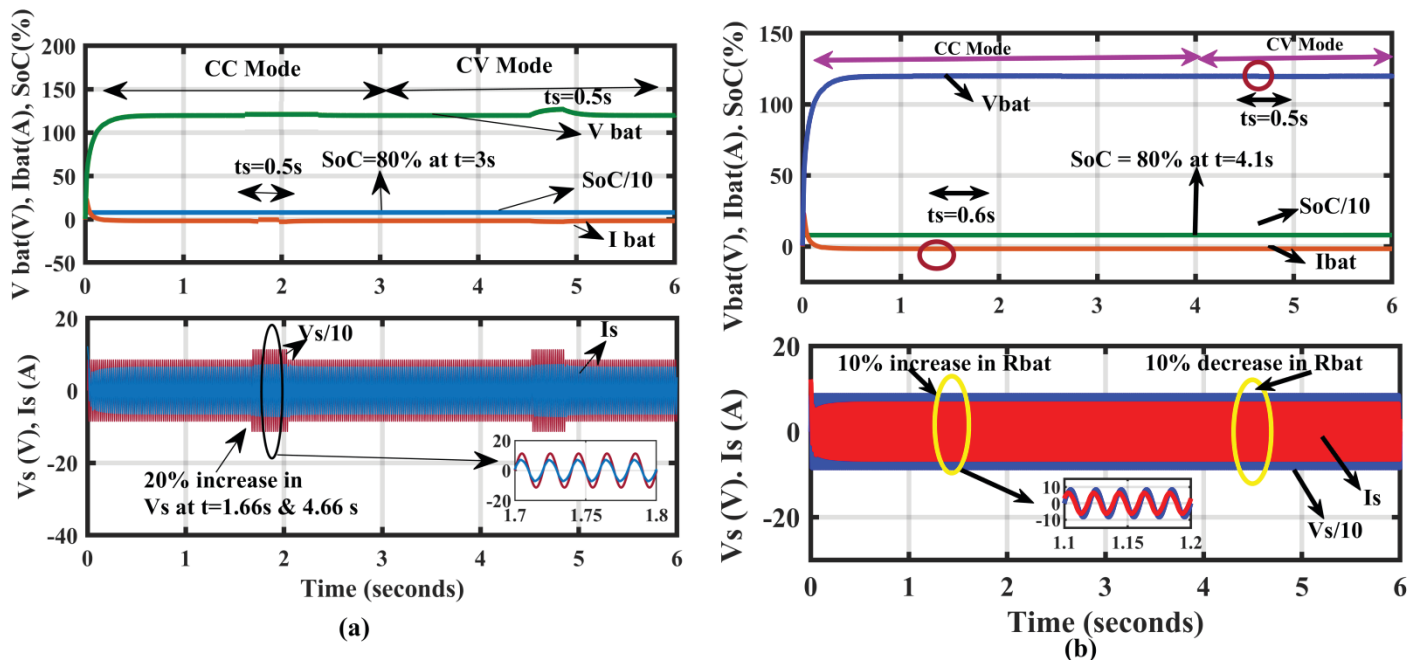


Figure 7. Performance evaluation under (a) Varying line (Grid fluctuations); and (b) Varying load (Battery internal resistance) conditions.

applications. Those batteries will be able to store up a large quantity of power in a small volume, making them suitable for defence applications. They can withstand numerous charge-discharge cycles, often ranging from 300 to 500 cycles or more, depending on the specific type and usage.

4.1 Battery Load – Rated Condition

A lithium-ion battery having a nominal voltage of 100V, rated capacity of 0.5 Ampere hr, and initial SoC – 79.7 % is used for simulation. Initially, the battery starts charging under CC mode, battery current reaches the final steady-state value with settling time $t_s = 0.25$ sec. Once SoC reaches 80 % at $t = 0.8$ sec., battery charging shifts to CV mode. Figure 6 demonstrates

the achievement of UPF (0.9996) operation with a THD of 2.6508 % and both during CC and CV mode of charging. The suggested GOA controller can produce controlled voltage in CV mode and regulated current in CC mode with sufficient robustness.

4.1 Performance Analysis Under Dynamic Conditions

4.1.1 Line Variations

To study about robustness of the GOA-tuned PI controller a 20 % increase in supply voltage (V_s) has been given at $t = 1.66$ seconds and a 20 % decrease in line voltage $t = 4.66$ sec. in both CC and CV modes respectively. The initial SoC is 79.5 %. CC to CV mode transition happens at $t = 3$ sec.

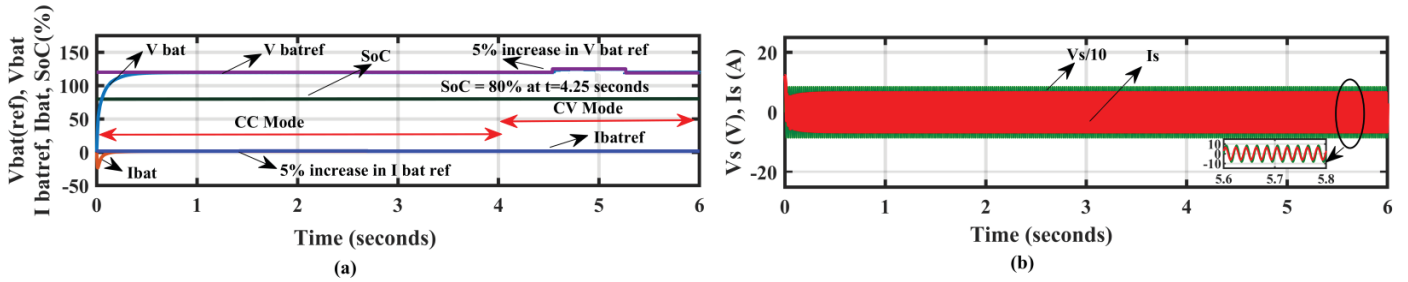


Figure 8. Simulation results for set point variations (a) Vbat, Ibat and SoC of the battery; and (b) Source voltage and source current.

Table 3. Comparison of performance metrics of conventional SEPIC and NIBS converter based PFC charger

Topology	Mode of operation	Performance indices							
		Rise time t_r (sec)	Peak time t_p (sec)	Peak overshoot (% Mp)	Settling time t_s (sec)	Steady-state error $e_{ss(t)}$	Power factor	THD (%)	Efficiency (%)
Single-stage (NIBS)	CC mode	0.154	0.364	9.15	0.454	0.026	0.9996	2.342	91.99
	CV mode	0.326	0.857	8.51	1.235	0.054			
Dual-stage (Conventional SEPIC)	CC mode	0.253	0.872	16.33	1.284	0.042	0.9954	9.612	86.88
	CV mode	0.675	0.945	14.56	1.572	0.067			

Figure 7(a) shows the battery voltage (Vbat), battery current (Ibat), and state of charge (SoC) operate in constant current (CC) and constant voltage (CV) modes, achieving near unity power factor (UPF) even when exposed to grid fluctuations.

4.1.2 Load Variations

To investigate the impact of load current variation, the battery's internal resistance (R_{bat}) was increased by 5 % at $t = 1.35$ sec. during CC mode. Subsequently, a 5 % decrease in internal resistance was applied at $t = 4.5$ sec. in CV mode. The initial SoC is 79.5 %. The CC to CV mode transition happens at $t = 4.15$ sec. when SoC reaches 80 %. Figure 7(b) shows the battery voltage (Vbat), battery current (Ibat), and state of charge (SoC) operate in constant current (CC) and constant voltage (CV) modes, achieving near unity power factor (UPF) even when there is a change in internal resistance of the battery (R_{bat}).

4.1.3 Set Point Variations

Figure 8(a) and (b) illustrates that GOA tuned PI controller tracks battery current reference in CC mode and battery voltage reference in CV mode with a settling time of 0.67 sec. and 1.25 sec. respectively. Thus, the UPF operation is maintained throughout the charging period with a source current harmonic distortion of 4.187 % and an input power factor of 0.9991. Table 3 shows the comparison between single-stage and dual-stage PFCs.

Table 4 shows a comparison between conventional SEPIC-based PFC chargers and NIBS converter-based chargers. Thus the NIBS PFC converter has fewer components compared to the conventional which results in elevated efficiency and, a reduction in the size of the charger.

Table 4. Comparison between conventional SEPIC and NIBS converter based PFC charger

Name of the component	NIBS converter	Conventional SEPIC
High-frequency diode	2	2
Fast recovery diodes	2	2
Line frequency diodes	2	4
Current conduction path		1 body diode, 2 line frequency diodes
• when L_1 is charging	1 line frequency diode, 1 body diode	1 fast switching diode, 2 line frequency diodes
• when L_1 is discharging	1 fast switching diode, 1 line frequency diode	

Table 5. Performance comparison of GA, PSO and GOA optimization Algorithms for tuning PI controller gain Values

Parameter	Algorithm		
	GA	PSO	GOA
Settling time (sec.)	1.89	1.25	0.56
Power factor	0.9354	0.9621	0.9996
THD (%)	5.654	5.172	2.6508
Load regulation (%)	0.8	0.6	0.1
Efficiency (%)	88.95	90.18	91.83

The performance of the proposed GOA based optimization technique is compared with existing optimization techniques like Genetic Algorithm (GA) and Particle Swarm Optimization (PSO). Simulation results reveal that the proposed GOA outperforms the GA and PSO in terms of various performance parameters listed in Table 5.

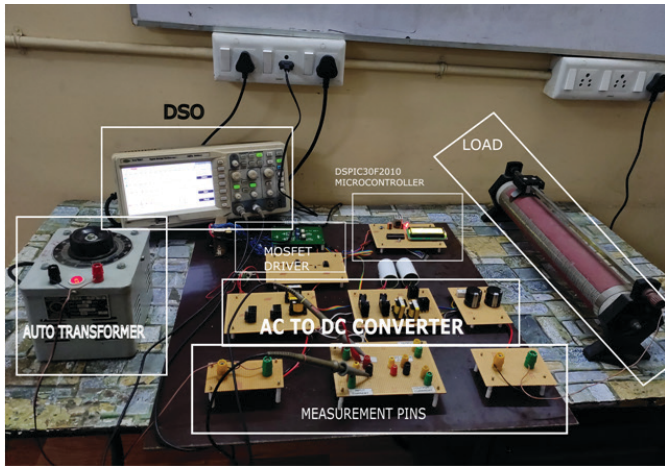


Figure 9. Experimental setup of 200 W NIBS converter.

5. EXPERIMENTAL RESULTS OF NIBS CONVERTER FEEDING A RESISTIVE LOAD

The experimental setup of 1 Φ AC-DC 200W NIBS converter controlled by GOA tuned outer PI voltage controller and inner current controller using DSPIC30F2010 microcontroller constructed is shown in the Fig. 9. The load voltage (DC), Rectified input voltage (V_{in}), inductor currents (i_{L1} and i_{L2}) is sensed, measured using sensor and scaled down inputs are fed to ADC of the microcontroller. The outer GOA tuned PI and inner predictive control algorithms are implemented by using DSPIC30F2010 microcontroller which generates the switching pulses for the MOSFET switches of the AC-DC NIBS PFC converter.

The closed-loop experimental results of NIBS Converter for outer GOA tuned PI controller for a resistive load is shown

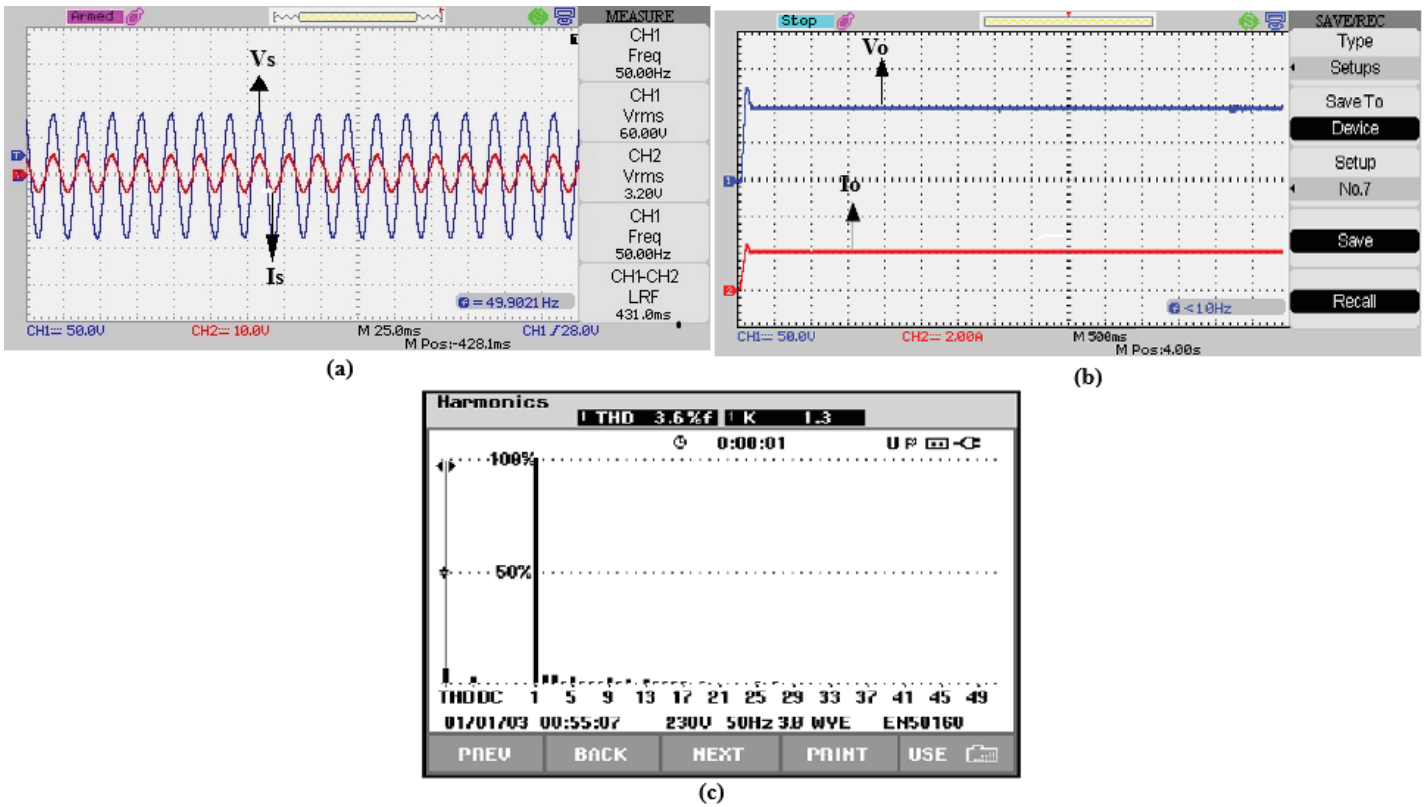


Figure 10. Experimental results for 200 W NIBS converter feeding a resistive load under rated condition (a) Source voltage and source current; (b) Load voltage and load current; and (c) THD spectrum of source current.

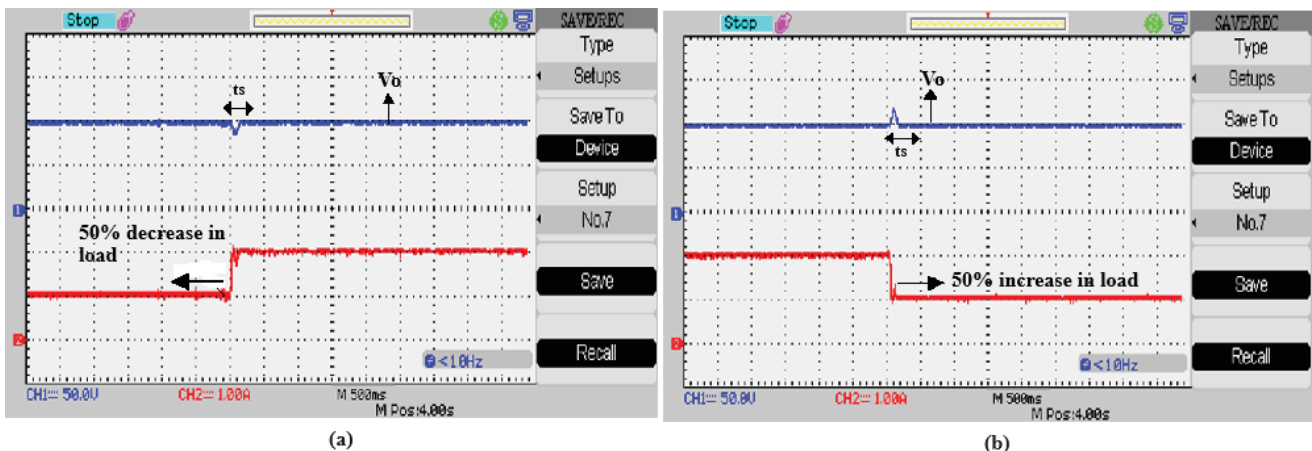


Figure 11. Experimental results for 200W NIBS converter under varying load condition.

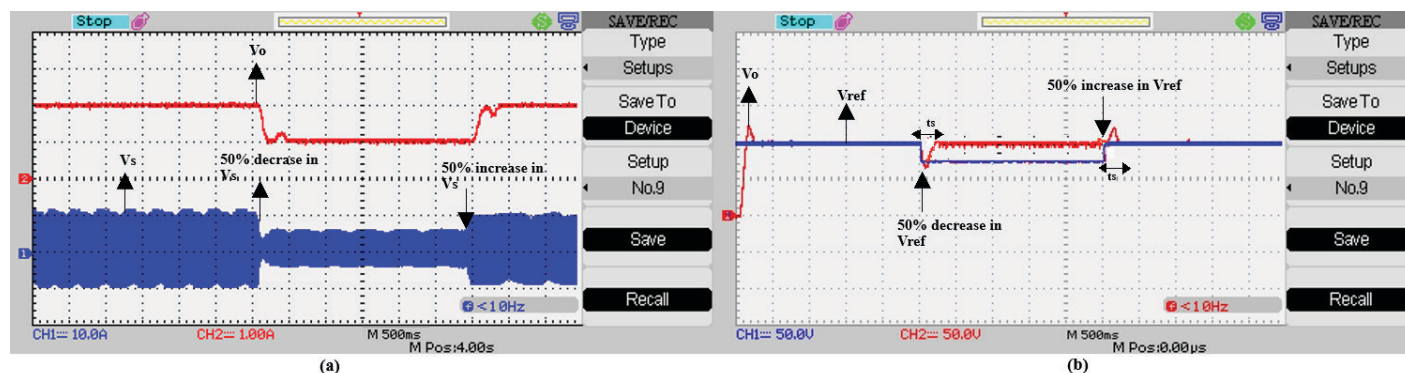


Figure 12. Experimental results for 200 W NIBS converter under (a) Varying source voltage; and (b) Servo operation.

in the Fig. 10. Figure 10 (a) ensures the UPF operation and Fig. 10 (b) represents the output load voltage (100V) and load current (2A). Figure 10 (c) shows the THD spectrum of the source current. Figure 11 shows the regulated voltage under load variations. Figure 11(a) representing decrease in load and Fig. 11(b) representing increase in load. Fig. 11(a) shows the source voltage variation and Fig. 12 (b) shows the servo operation.

6. CONCLUSION

The design and implementation of a 1 Φ AC-DC NIBS converter for PFC and regulated output for battery charging applications has been presented. A seventh-order NIBS converter model was simplified to a third-order system through Hankel matrix reduction, focusing on critical state variables for optimal PFC and output regulation in battery charging applications. Outer and inner PI controller parameters K_p and K_i are tuned using the GOA controller for battery load. Controller performance

has been validated for its resilience to fluctuations in load resistance, line voltage, and desired value. Operational metrics of the NIBS converter demonstrate near-unity power factor operation, Improvement in efficiency; and reduced THD for battery charging. The recommended GOA controller can produce controlled voltage in CV mode and controlled current in CC mode with sufficient sturdiness in batteries. They are crucial for the efficient, reliable, and versatile power management required in EVs for defence applications. Their ability to provide stable, regulated power in a compact and efficient form factor makes them indispensable for modern military applications.

REFERENCES

- Lam, L. & Bauer, P. Practical capacity fading model for Li-Ion battery cells in electric vehicles, *IEEE Trans. Pow. Elec.*, 2013, **28**(12), 5910-5918. doi: 10.1109/TPEL.2012.2235083
- Liu, Z.; Li, Y.; Wang, Q. & Li, J. TSCW-GAN based FDIAs defence for state-of-charge estimation of battery energy storage systems in smart distribution networks. *Sci. J.*, 2023, **20**(4), 5048-5059. doi: 10.1109/TII.2023.3331544
- Ma, Q.; Wei, W.; Wu, L. & Mei, S. Life-aware operation of battery energy storage in frequency regulation, 2023, *IEEE Trans. Sus. Ene.*, **14**(3), 1725-1736, doi: 10.1109/TSTE.2023.3245197.
- Satyavani, T.; Rao, G.; Kumar, A. & Rao, K. Study of electrical and thermal behaviour of Li-ion polymer cells for auxiliary power supply in underwater applications. *Sci. J.*, 2012, **62**(2), 127-131. doi:10.14429/dsj.62.995
- Sayed. S.S. & Massoud, A.M. Review on state-of-the-art unidirectional non-isolated power factor correction converters for short-/long-distance electric vehicles. *IEEE Acc.*, 2022, **10**, 11308-11340. doi: 10.1109/ACCESS.2022.3146410.
- SAE International. Electric vehicle and plug-in hybrid electric vehicle conductive charge coupler. SAE J1772:2010, Warrendale, PA, USA, 2010.
- Pandey, R. & Singh, B. A power factor corrected resonant EV charger using reduced sensor-based bridgeless boost PFC converter. *IEEE Trans. Ind. Appl.*, 2021, **57**(6), 6465-6474. doi:10.1109/TIA.2021.3106616.
- Dadhaniya, P.; Maurya, M. & Vishwanath, G.M. A bridgeless modified boost converter to improve power factor in EV battery charging applications. *IEEE J. Emerg. Sel. Top. Ind. Electron.*, 2024, **5**(2), 553-564. doi:10.1109/JESTIE.2024.3355887.
- Jang, Y. & Jovanovic, M.M. Bridgeless high-power-factor buck converter. *IEEE Trans. Pow. Elec.*, 2011, **26**(2), 602-611. doi: 10.1109/TPEL.2010.2068060
- Zhao, B.; Abramovitz, A. & Smedley, K. Family of bridgeless buck-boost PFC rectifiers. *IEEE Trans. Pow. Elec.*, 2015, **30**(12), 6524-6527. doi: 10.1109/TPEL.2015.2445779
- Liu, X.; Xu, J.; Chen, Z. Single-inductor dual-output buck-boost power factor correction converter. *IEEE Trans. Ind. Elec.*, 2015, **62**(2), 943-952.
- Singh, A.K.; Mishra, A.K.; Gupta, K.K. & Kim, T. Comprehensive review of non-isolated bridgeless power factor converter topologies. *IET Cir. Dev. Sys.*, 2021, **15**, 197-208. doi: 10.1049/cds2.12046
- Spiazzi, G. & Mattavelli, P. Design criteria for power factor preregulators based on SEPIC and Cuk converters in continuous conduction mode. *In Proceedings of the*

- IEEE Industry Applications Society Annual Meeting, IEEE, Denver, CO, USA, 1994, **2**, 1084–1089.
doi: 10.1109/IAS.1994.377563.
14. Kushwaha, R.; Singh, B. & Khadkikar, V. An isolated bridgeless cuk–SEPIC converter-fed electric vehicle charger. *IEEE Trans. Ind. App.*, 2022, **58**(2), 2512–2526.
doi: 10.1109/TIA.2021.3136496
 15. Durgadevi, S. & Umamaheswari, M.G. Analysis and design of single phase power factor correction with DC-DC SEPIC converter for fast dynamic response using genetic algorithm optimized PI controller. *IET Cir., Dev. & Sys.*, 2018, **12**(2), 164–174.
doi: 10.1049/iet-cds.2017.0229.
 16. Mahdavi, M. & Farzanehfard, H. Bridgeless SEPIC PFC rectifier with reduced components and conduction losses. *IEEE Trans. Ind. Elec.*, 2011, **58**(9), 4153–4160.
doi: 10.1109/TIE.2010.2095393.
 17. Gupta, J. & Singh, B. A single-stage bridgeless isolated AC–DC conversion system for light electric vehicles charging application. *IEEE Trans. Trans. Elec.*, 2023, **9**(1), 1379–1389.
doi: 10.1109/TTE.2022.3193314
 18. Sree, B.L. & Umamaheswari, M.G. A hankel matrix reduced-order SEPIC model for simplified voltage control optimization and MPPT. *Sol. Ene.*, 2018, **170**, 280–292.
doi: 10.1016/j.solener.2018.05.059.
 19. Vishwakarma, C.B. Modified hankel matrix approach for model order reduction in the time domain. *Int. J., Phy., & Math. Sci.*, 2014, **8**(2), 404–410.
doi: 10.5281/zenodo.1091386
 20. Gopal J., N. & N.B., Muthuselvan. Current mode fractional order PID control of wind-based quadratic boost converter inverter system with enhanced time response. *Cir. Wor.*, 2021, **47**(4), 368–381.
doi: 10.1108/CW-03-2020-0038
 21. International Electrotechnical Commission. Limits for Harmonic Current Emissions. IEC 61000-3-2, Geneva, Switzerland, 2000.
 22. Gopal, J.N.; Natarajan, B.M. & Muthukaruppasamy, S. Model predictive controller–based quadratic boost converter for WECS applications. *Int. Trans. Elec. Ene. Sys.*, 2021, **31**(12), e13133.
doi:10.1002/2050-7038.13133
 23. Meraihi, Y.; Gabis, A.B.; Mirjalili, S. & Ramdane-Cherif, A. Grasshopper optimization algorithm: Theory, variants, and applications. *IEEE Acc.*, 2021, **9**, 50001–50024.
doi: 10.1109/ACCESS.2021.3067597
 24. Saremi, S.; Mirjalili, S. & Lewis, A. Grasshopper Optimisation algorithm: Theory and application. *Adv. Engg. Soft.*, 2017, **105**, 30–47.
doi: 10.1016/j.advengsoft.2017.01.004
 25. Komathi, C. & Umamaheswari, M.G. Analysis and design of genetic algorithm-based cascade control strategy for improving the dynamic performance of interleaved DC–DC SEPIC PFC converter. *Neu. Comp. & App.*, 2020, **32**, 5033–5047.
doi: 10.1007/s00521-018-3944-9
 26. Eswaran, T. & Kumar, V.S. Particle swarm optimization (PSO)-based tuning technique for PI controller for management of a distributed static synchronous compensator (DSTATCOM) for improved dynamic response and power quality. *J. App. Res. & Tech.*, 2019, **15**(2).
doi: 10.1016/j.jart.2017.01.011

CONTRIBUTORS

Mrs K.M. Vijayalakshmi obtained her M.E. degree in PED from Anna University, Chennai, Tamil Nadu, India and working as an Assistant Professor at Department of Electrical and Electronics Engineering, Rajalakshmi Engineering College. Her areas of interest include: Power electronic converters, renewable energy systems and Electric Vehicle battery charging applications. Contribution in the current study: Modelling of NIBS converter, design of NIBS converter and GOA tuned PI Controller, closed-loop simulation using GOA tuned PI controller, hardware implementation of NIBS converter and preparation of the manuscript.

Dr M.G. Umamaheswari obtained PhD in the area of power quality from College of Engineering, Anna University, Chennai and working as a Professor at Department of Electrical and Electronics Engineering, Rajalakshmi Engineering College. Her areas of interest include: Power quality enhancement using power converters and, the application of linear and nonlinear controllers to renewable power-fed converters. Contribution in the current study: Problem formulation, Verification of NIBS converter and GOA tuned PI controller Design, verification of simulation & hardware results, and verification of the manuscript draft.